Nanoscale

PAPER

View Article Online
View Journal | View Issue

Cite this: *Nanoscale*, 2017, **9**, 362

Nanoconfined self-assembly on a grafted graphitic surface under electrochemical control†

Thi Mien Trung Huynh,*‡[a,b] Thanh Hai Phan,‡[a,c] Oleksandr Ivasenko,[a] Stijn F. L. Mertens*[a,d] and Steven De Feyter*[a]

Received 23rd September 2016,
Accepted 29th November 2016

DOI: 10.1039/c6nr07519c

www.rsc.org/nanoscale

Highly oriented pyrolytic graphite (HOPG) can be covalently grafted with aryl radicals generated *via* the electrochemical reduction of 3,5-bis-*tert*-butyl-diazonium cations (3,5-TBD). The structure of the grafted layer and its stability under electrochemical conditions were assessed with electrochemical scanning tunneling microscopy (EC-STM) and cyclic voltammetry (CV). Stable within a wide (>2.5 V) electrochemical window, the grafted species can be locally removed using EC-STM-tip nanolithography. Using dibenzyl viologen as an example, we show that the generated nanocorrals of bare graphitic surface can be used to study nucleation and growth of self-assembled structures under conditions of nanoconfinement and electrochemical potential control.

Introduction

Graphene is a one-atom-thick carbon sheet and is considered to be the thinnest, strongest, and stiffest material currently known.[1,2] Since the first experimental evidence of a free-standing monolayer sheet in 2004, graphene has garnered tremendous scientific interest due to its unique electronic, optical, mechanical and thermal properties, where it outperforms most other materials.[2,3] Despite these exceptional qualities, certain aspects impede a straightforward implementation. For instance, the zero-bandgap of graphene, responsible for its excellent electrical conductivity, leads to a very small on/off ratio in graphene based field effect transistors.[3] Another issue is its low solubility that has an impact on the ease of processing.

Molecular functionalization of graphene addresses these challenges, and is a promising approach to widen the scope of its applications, such as in electronic devices, biosensors and composite materials.[4] Both non-covalent and covalent functionalization protocols of graphitic surfaces have been explored extensively.[5–17] The non-covalent approach relates to the physisorption of molecules, and in specific cases, organic molecules self-assemble into 2D crystalline films on top of the graphitic surface. Physisorption may alter the carrier concentration of graphene without affecting its materials properties.[12,13,18] In contrast, covalent grafting results in band-gap opening near the Fermi level of graphene, turning pristine "metallic" graphene into a "semiconductor".[5,7–9,11,16]

The most widely used procedure for covalent modification of graphitic surfaces involves the electroreduction of aryldiazonium salts.[16,17,19–28] Electrons are transferred from the carbon surface to the diazonium cations at the solid–liquid interface. The release of a dinitrogen molecule results in a radical species that can attack the sp^2 carbon lattice and be anchored there *via* covalent bond formation. Two major shortcomings of diazonium chemistry are the limited grafting density in combination with dendritic multilayer formation.[22,23,26] As we recently demonstrated,[16] both problems can be solved by grafting the sterically hindered 3,5-TBD, yielding high-density yet strict monolayer growth.[16,19,20,24,26,27]

For many applications, the stability of the grafted film is an important issue. The thermal and solvent stability of various grafted films on carbon-based and metallic surfaces has been reported.[29–31] However, to the best of our knowledge, the *in situ* structural characterization at the nanoscale of grafted films and their stability under electrochemical control have not yet been reported.

[a]*KU Leuven-University of Leuven, Department of Chemistry, Division of Molecular Imaging and Photonics, Celestijnenlaan 200F, B-3001 Leuven, Belgium. E-mail: steven.defeyter@kuleuven.be, huynhthimientrung@qnu.edu.vn, stmerten@gmail.com*

[b]*Quy Nhon University, Department of Chemistry, 170 An Duong Vuong, Quy Nhon, Vietnam*

[c]*Quy Nhon University, Department of Physics, 170 An Duong Vuong, Quy Nhon, Vietnam*

[d]*Institute of Applied Physics, Vienna University of Technology, Wiedner Hauptstraße 8-10/E134, A-1040 Vienna, Austria*

†Electronic supplementary information (ESI) available. See DOI: 10.1039/c6nr07519c

‡These authors contributed equally to this work.

We have recently developed a protocol for the creation of nanoconfined areas (nanocorrals) based on STM tip manipulation of these covalently modified graphitic surfaces, and provided proof-of-concept evidence for the self-assembly of a long-chain molecule, pentacontane, in those nanocorrals, at the interface between an organic solvent and the substrate.[16] While in-depth studies are still in progress, we believe that confining the self-assembly of functional organic molecules within the corrals may lead to new structures and properties. It is, therefore, useful to explore and apply this concept to the self-assembly of electroactive organic molecules under electrochemical control.

As a representative example thereof, viologens have attracted much attention in the field of surface electrochemistry as they can be applied as chromophores, electron-transfer mediators and gating molecules.[32–34] The reduced, uncharged species (V^0), has been recently recognized as n-dopant for various carbon nanostructures including nanotubes[35] and graphene[11,36] as well as for other 2D materials such as MoS_2.[37] However, while reduced viologen has been synthesized for doping purposes, *in situ* electrochemical generation of viologen-doped 2D materials *via* the self-assembly approach has not been reported so far.

In this study, the diazonium grafting process on graphite and the stability of the grafted films as a function of electrode potential are investigated using cyclic voltammetry and EC-STM. Further, we show that it is possible, under electrochemical control, to locally degraft molecules *via* EC-STM tip based nanomanipulation. In the process, nanocorrals of pristine graphite surface are generated, in which reduced viologen molecules can self-assemble under electrochemical control. This experimental finding opens new avenues to investigate supramolecular self-assembly of n-/p-doping molecules in nanoconfined spaces under electrochemical control towards bottom-up creation of nanoconfined n-/p-doped 2D materials for nanoscale electronics applications.

Experimental

3,5-Bis-*tert*-butyl-aniline was purchased from TCI-Tokyo Chemical Industry Co., Ltd, and dibenzyl viologen (DBV) from Sigma-Aldrich; both compounds were used without further purification. High purity water (Milli-Q, Millipore, TOC < 3 ppb, 18.2 MΩ cm) was used for electrolyte preparation, including the supporting electrolyte (50 mM HCl), 3,5-TBD containing electrolyte (2 mM 3,5-bis-*tert*-butyl-aniline + 50 mM HCl + excess 0.1 M $NaNO_2$) and the DBV containing electrolyte (0.1 mM DBV + 50 mM HCl). All electrolytes were deoxygenated with argon gas (grade 5.0, Praxair) for several hours before use. 3,5-Bis-*tert*-butyl-diazonium (3,5-TBD) was generated immediately before grafting by adding a small excess of 0.1 M $NaNO_2$ to the aniline precursor dissolved in 50 mM HCl, and stirring for 2 minutes before injection into the electrochemical cell.

All CV measurements were performed employing an Autolab PGSTAT101 potentiostat (Metrohm-Autolab BV, the Netherlands). Prior to each experiment, the HOPG electrode (ZYB grade, Momentive Performance Materials) was freshly cleaved using scotch tape. The electrochemical grafting of 3,5-TBD on HOPG was carried out in a lab-built single-compartment three-electrode cell, exposing a geometric working electrode area of 38.5 cm^2. Pt wire and Ag/AgCl/3 M NaCl served as counter and reference electrodes, respectively. All potentials are reported *versus* the reversible hydrogen electrode (RHE). During the measurements, the electrolyte was kept under Ar. After grafting, the 3,5-TBD modified HOPG sample was rinsed with hot toluene and Milli-Q-water to remove physisorbed material from the surface, and finally dried with a stream of nitrogen before being transferred to the EC-STM cell.

All EC-STM experiments were carried out with an apparatus designed at the University of Bonn as described elsewhere;[38] relevant potentials are defined in Fig. 1a. In order to eliminate the influence of oxygen as well as acoustic and electromagnetic interference, the entire EC-STM system is housed in a sealed aluminum chamber with electrical and liquid feedthroughs and filled with Ar. The STM tips were electrochemically etched from 0.25 mm tungsten wire in 2 M KOH solution, rinsed with water, dried and subsequently coated by passing the tip through a lamella of hot-melt glue.

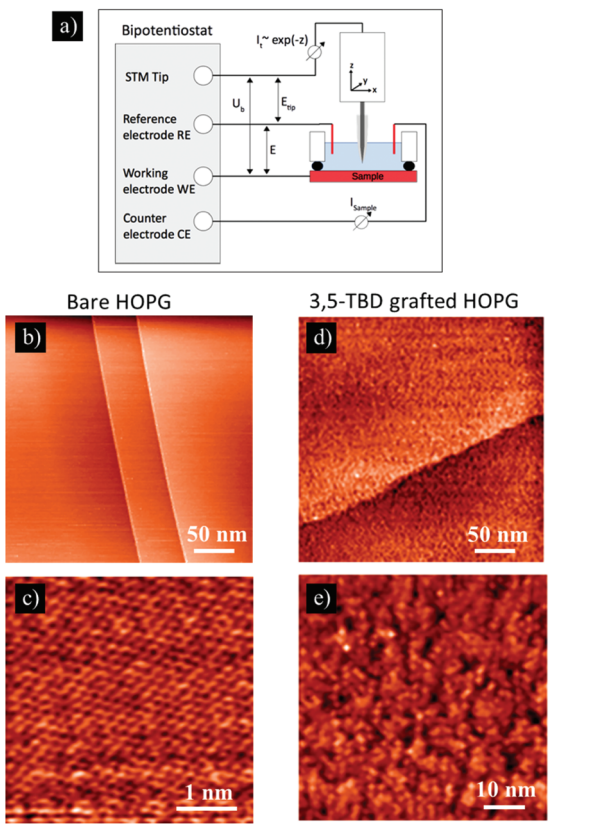

Fig. 1 (a) Schematic EC-STM setup. EC-STM images of (b–c) bare HOPG and (d–e) of 3,5-TBD covalently grafted HOPG. Imaging parameters: (b) substrate potential E = +100 mV, sample bias U_b = −150 mV, setpoint current I_t = 0.2 nA; (c) E = +100 mV, U_b = −20 mV, I_t = 1.2 nA; (d–e) E = +147 mV, U_b = −179 mV, I_t = 0.2 nA.

Results and discussion

Electrochemical grafting of diazonium on HOPG

Covalent functionalization of HOPG by diazonium radicals using electrochemical method has been described in detail elsewhere.[16] An overview of this process is provided in Fig. S1.†

The efficiency of the grafting process is characterized by EC-STM measurements. Fig. 1 shows large scale and high resolution EC-STM images of bare HOPG (Fig. 1b and c) and 3,5-TBD grafted HOPG (Fig. 1d and e). All images were recorded in 50 mM HCl. Since chloride anions hardly adsorb on HOPG,[39] high-resolution STM images reveal the typical hexagonal structure of bare HOPG (Fig. 1c), whereas a high-density monolayer is observed after the electrochemical reduction and grafting of the 3,5-TBD species. This result is in line with STM observations under ambient conditions, as reported earlier.[16] The presence of the *tert*-butyl groups at the *meta*-positions of the phenyl ring prevents the growth of multilayers, which otherwise readily form by the attachment of generated radicals onto those positions.[16,27]

Electrochemical stability of the covalently grafted layer

The influence of the applied potential on the stability of the grafted 3,5-TBD species on HOPG was examined using a combination of cyclic voltammetry and EC-STM.

Fig. 2 shows the CVs of bare HOPG (red curve) and 3,5-TBD grafted HOPG (black curve) in 50 mM HCl. In the double layer region (Fig. 2, inset), grafting decreases further the low interfacial capacitance of HOPG. The potential window of bare HOPG in HCl solution is limited by the oxygen evolution reaction (OER) at the anodic limit and the hydrogen evolution reaction (HER) at the cathodic limit. The presence of the grafted layer on the graphitic surface is seen to shift the onset of both OER and HER. Compared to bare HOPG, the HER on 3,5-TBD grafted HOPG surface starts 190 mV more negative than on bare HOPG whereas the OER onset is shifted positively by 240 mV. The change in onset of both OER and HER is constant upon multiple cycling (Fig. S2†). This observation may indicate the blocking effect of active sites on HOPG by 3,5-TBD for both reactions, or may find its origin in an increase of ohmic potential drop across the grafted layer. This effect was also reported for HOPG and metal electrode surfaces that were non-covalently functionalized by organic thin films.[40,41]

EC-STM measurements were used to verify the stability of the 3,5-TBD grafted layer on HOPG as a function of substrate potential. Fig. 3 shows a series of STM images that was recorded at the same grafted surface area while the applied potential was altered within the full potential window. The grafted layer of 3,5-TBD on HOPG remains intact at all potentials including OER and HER potential regimes, and no signs of 3,5-TBD desorption were observed. The strong covalent bond between grafted 3,5-TBD and the carbon lattice is thus impervious to the effects of cycling in the entire available potential window.

The electrochemical stability of the grafted layer is further demonstrated by the response of a hexacyanoferrate redox probe, which on freshly exfoliated HOPG shows reversible behaviour.[42] Accordingly, CVs of 3,5-TBD/HOPG were measured in 1 mM $K_3Fe(CN)_6$ + 0.2 M Na_2SO_4 after polarization of the electrode for 3 min at −800 mV, 0 mV, +800 mV and +1400 mV in 50 mM HCl, Fig. 4. The presence of the non-conductive grafted layer blocks the electron transfer between HOPG electrode and the $Fe(CN)_6^{3-}$ species at the solid/liquid interface.[43] No matter how far the potential excursion is extended, the electron transfer blocking behavior of the 3,5-TBD-modified HOPG remains intact.[29]

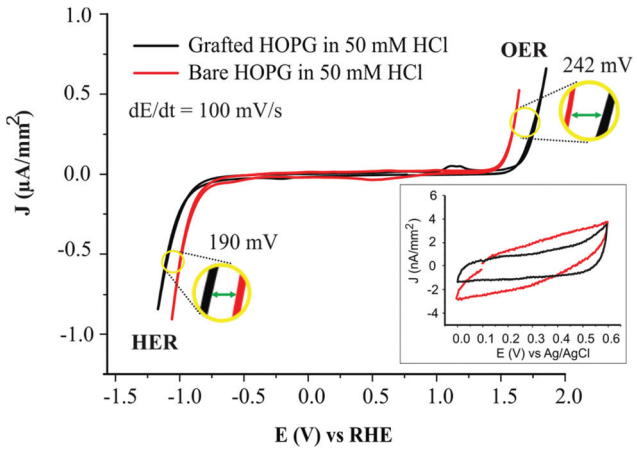

Fig. 2 Cyclic voltammograms of bare HOPG (red curve) and 3,5-TBD modified HOPG (black curve) in 50 mM HCl reveal an enlarged potential window between the onset of HER and OER for the grafted surface. The inset compares the double layer region of bare and grafted HOPG.

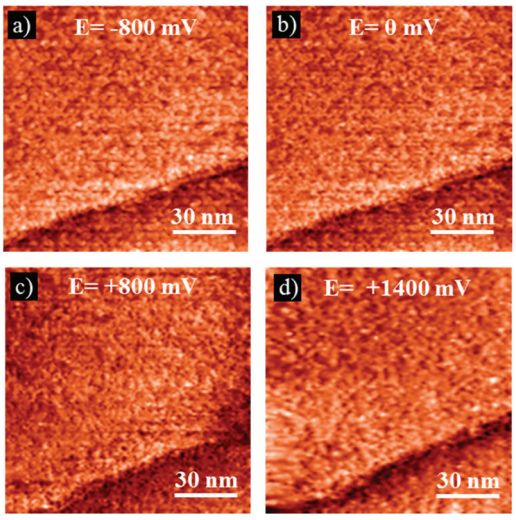

Fig. 3 Series of STM images recorded at the same grafted surface area as a function of substrate potential, as indicated in the images, showing the electrochemical stability of the 3,5-TBD grafted layer: (a–d) U_b = −150 mV, I_t = 0.15 nA.

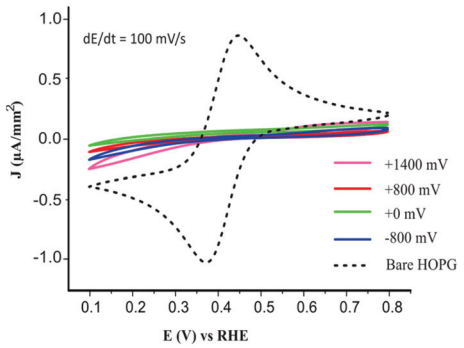

Fig. 4 CVs of bare HOPG (dashed-black trace) and 3,5-TBD grafted HOPG in 1 mM $K_3Fe(CN)_6$ + 0.2 M Na_2SO_4 after polarization for 3 min at −800 mV (blue trace), 0 mV (green trace), +800 mV (red trace) and +1400 mV (pink trace) in 50 mM HCl.

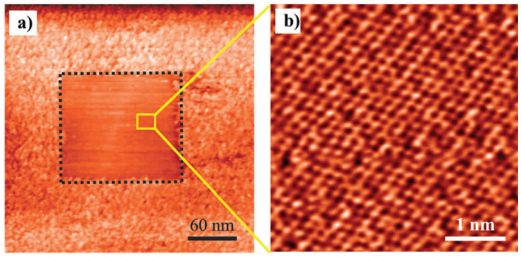

Fig. 5 (a) EC-STM tip assisted nanocorral creation on 3,5-TBD grafted HOPG surface at E = −50 mV. The scanning parameters used for nanoshaving: U_b = −20 mV; I_t = 2 nA, and for imaging after nanoshaving: U_b = −200 mV; I_t = 0.1 nA; (b) high resolution of hexagonal HOPG lattice after nanoshaving: U_b = −10 mV; I_t = 1.2 nA.

The combined EC-STM and CV results indicate that the covalently grafted 3,5-TBD layer on HOPG is highly stable against changes in the electrochemical potential. This finding opens the possibility of using the grafted layer as a robust mask to drive the selective self-assembly within nanocorrals of electroactive organic molecules under electrochemical control.

EC-STM tip nanolithography and molecular self-assembly within nanocorrals

The concept of STM tip-assisted lithography and nanomanipulation on functionalized solid surfaces is well documented, in particular for thiol based molecular layers self-assembled on gold.[30,44–48] Few experiments deal with tip-based degrafting of molecules on graphite or graphene and most of them were carried out under UHV conditions.[6,49] Under ambient conditions, we recently demonstrated such degrafting by tip-assisted nanoshaving of covalently grafted 3,5-TBD on HOPG and CVD graphene on Cu.[16] The regeneration of the pristine graphitic substrate, *i.e.* the conversion of the graphitic surface from the distorted sp^3 configuration back to original sp^2 lattice, was also demonstrated. Importantly, no differences between degrafted areas and freshly exfoliated HOPG could be detected using high-resolution STM, Raman microscopy or self-assembly behavior. *In situ* nanoshaving at the solid–liquid interface results in the exposed substrate surface becoming host to molecular self-assembly.[16,50] However, to the best of our knowledge, degrafting in an EC-STM setup and self-assembly under electrochemical control within degrafted areas has not been demonstrated.

Fig. 5 illustrates the degrafting process at an HOPG–electrolyte interface by employing the EC-STM tip. The grafted layer is almost unaffected by the EC-STM tip under mild tunneling imaging conditions, *i.e.* high bias voltage and low tunneling current. However, grafted molecules are removed under more drastic tunneling conditions, *i.e.* low bias voltage and high tunneling current, leaving a corral free from grafted molecules behind as marked by the dashed square in Fig. 5a. The surface morphology (Fig. 5a) and high-resolution image (Fig. 5b) of the degrafted corral are similar to that of bare HOPG shown in Fig. 1b and c. This finding suggests that also EC-STM tip based degrafting converts the sp^3 hybridization back to original sp^2 pristine graphite lattice, which concurs with our previous study.[16]

Our experimental results demonstrate that also the EC-STM tip can act as a "nanoshaver" to locally remove covalently grafted molecules from HOPG. The as-formed degrafted areas are prone to functionalization under electrochemical control such as supramolecular self-assembly. The advantage over both UHV and ambient conditions is that electrochemical conditions allow strong control over adsorption/desorption processes and phase transition of molecules.

To illustrate this concept, we explored the self-assembly of dibenzyl viologen (DBV) in the nanocorrals. This molecule (Fig. 6a) is a redoxactive compound possessing three redox states, *viz.* dication (DBV^{2+}), monocation (DBV^{+}) and uncharged form (DBV^0). The redox states of DBV can be reversibly converted by proper selection of the electrochemical potential (Fig. S3†).[51,52]

Fig. 6 shows STM images recorded in 0.1 mM DBV + 50 mM HCl, immediately following tip-assisted degrafting. Note that degrafting itself took place in the presence of the same electrolyte. During degrafting, the substrate potential was kept at E_1 = −300 mV (Fig. 6b–d) or E_2 = −510 mV (Fig. 6e–g), where DBV is expected to occur in its radical monocationic ($DBV^{\bullet+}$) and uncharged form (DBV^0), respectively (see Fig. S3†). As seen from Fig. 6, immediately following the nanocorral formation, the reduced viologen species selectively self-assemble within the nanocorrals and form different ordered structures at different substrate potentials. The size of the self-assembled monolayer is determined by the dimensions of the degrafted nanocorrals. We note that the defect density in the self-assembled layers inside the nanocorrals is higher than on standard HOPG surfaces (see Fig. S7a and b†). We propose that this difference is a direct expression of the nanoconfinement itself: the very small domains that can form in the corrals do so under very different conditions from the large domains on unrestricted HOPG surfaces, where Ostwald-like ripening takes place and large domains grow at the expense of smaller domains, leading to longer-range order. Also, nucleation is expected to take place primarily at the edges of the

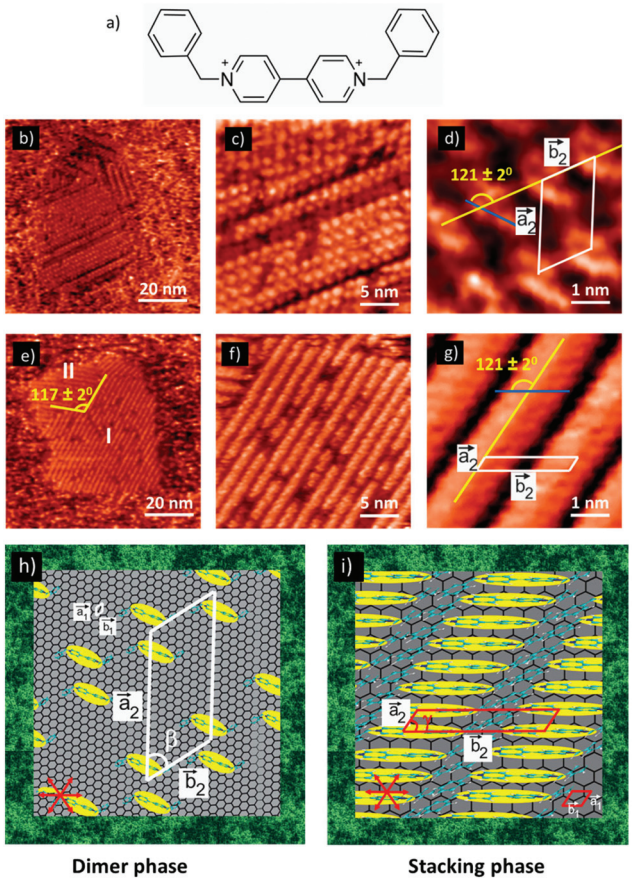

Fig. 6 (a) Chemical structure of dibenzyl viologen. (b–i) Substrate potential dependent formation of self-assembled monolayers within degrafted nanocorrals; (b–d) nanoconfined dimer phase: E_1 = −300 mV, U_b = +200 mV, I_t = 0.1 nA, $|\overrightarrow{a_2}| = 2.6 \pm 0.4$ nm, $|\overrightarrow{b_2}| = 1.6 \pm 0.3$ nm, β = 60° ± 4°; (e–g) nanoconfined stacking phase: E_2 = −510 mV, U_b = +330 mV, I_t = 0.1 nA, $|\overrightarrow{a_2}| = 0.6 \pm 0.4$ nm, $|\overrightarrow{b_2}| = 2.5 \pm 0.4$ nm, $\gamma = 59° \pm 4°$; tentative models of (h) dimer phase and (i) stacking phase.

nanocorral, whose length/area ratio is much higher than on an open surface. The difference in behaviour in our opinion underscores the added value of our approach, as much may be learned about nucleation and growth of self-assembled structures by providing restricted substrate areas.

At E_1 = −300 mV, each bright feature is believed to consist of two individual radical monocations ($DBV^{\bullet+}$) forming a so-called "dimer phase" as shown in Fig. 6b–d. By contrast, the DBV^0 uncharged species forms a stacking phase at E_2 = −510 mV as shown in Fig. 6e–g. Different domains are rotated with respect to each other by 117 ± 2° (Fig. 6e). Individual $DBV^{\bullet+}$ and DBV^0 species appear as elongated features (blue lines), which align face-to-face due to π–π interactions between neighboring benzyl groups and spin pairing between neighboring reduced bipyridinium.[52] Strikingly, in both the dimer and the stacking phases, individual molecules are rotated with respect to the long row axis (yellow lines) by 121 ± 2° (Fig. 6d and g) suggesting the influence of the graphite substrate in directing the self-assembly. The orientation of the molecular rows and of the individual species within the rows in both phases runs parallel to the symmetry axes of the underlying hexagonal HOPG lattice as observed with respect to bare HOPG (Fig. S4 and S5†). Tentative models for the respective phases are shown in Fig. 6h and i.

The dynamics of molecular phase transitions on changing the substrate potential was also experimentally observed. Fig. 7 shows the same surface area in response to shifting the substrate potential to more negative values. The dimer phase (Fig. 7a) is persistent in the potential regime −420 mV < E < −280 mV, and assigned to the formation of $DBV^{\bullet+}$ (Fig. S3†). On passing the second reduction peak ($DBV^{\bullet+} \rightarrow DBV^0$) at E = −450 mV, this ordered phase is gradually broken down and the stacking phase of DBV^0 partially appears. The phase transition starts at the borders of the nanocorral, which is therefore identified as a nucleation center (yellow arrow in Fig. 7b). A complete phase conversion is obtained when the substrate potential reaches E = −520 mV (Fig. 7c). Interestingly, a structural optimization of the stacking phase is also observed by ripening of domain size and orientation as indicated by yellow arrows in Fig. 7d. The dimer-to-stacking phase transition within the nanocorrals is a reversible process: sweeping the substrate potential back in positive direction leads to the reappearance of the dimer structure corresponding to the conversion of DBV^0 to $DBV^{\bullet+}$ (Fig. S6†). At potentials E > −280 mV, dicationic DBV^{2+} is formed, which binds only weakly to HOPG[53] and results in a 2D adsorbate gas phase instead of an ordered structure (see Fig. S7c†).

The self-assembly of DBV on HOPG under electrochemical conditions has been studied previously, albeit in a different electrolyte.[53] The voltammetric behavior in that case was limited to one pair of sharp peaks, indicative of a faradaic phase transition between the 2D adsorbate gas and the stacking phase, which was assigned to $DBV^{\bullet+}$. In the present case,

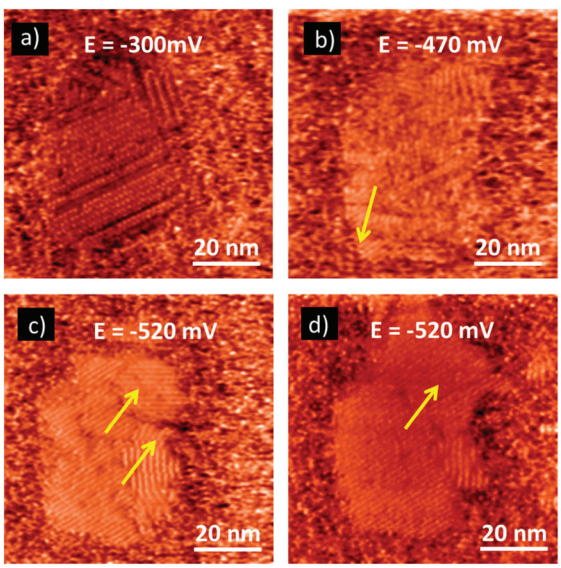

Fig. 7 Dynamics of phase transition of the viologen molecule driven by change in substrate potential. U_b = +150 mV, I_t = 0.1 nA.

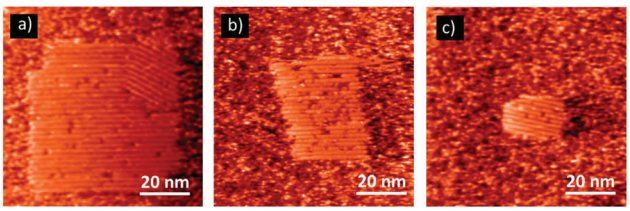

Fig. 8 Self-assembly of DBV^0 within nanocorrals of different size created by the EC-STM tip, E = −530 mV, U_b = +230 mV, I_t = 0.1 nA.

the voltammogram clearly shows a third stability region in the cathodic scan (see Fig. S3†), where the dimer phase is observed ($DBV^{\bullet+}$), before the stacking phase (DBV^0) is reached at the most negative potentials.

Nanocorrals of three different sizes were constructed (57 nm × 57 nm, 42 nm × 34 nm and 30 nm × 20 nm, Fig. 8) and the self-assembly of DBV^0 (stacking phase) was monitored. In these proof-of-concept experiments, self-assembly is observed irrespective of the size of the nanocorrals. This level of control over the size and shape of nanocorrals will allow investigating nucleation and monolayer growth processes in nanoconfined spaces under electrochemical control.

Conclusions

Cyclic voltammetry and EC-STM were combined to study the formation of 3,5-TBD based monolayers covalently grafted on the basal plane of HOPG, and to evaluate their stability against electrode potential cycling. The grafted monolayer blocks the electron transfer at the graphitic substrate and shifts the onset of the HER and OER. In addition, the EC-STM tip can act as nanoshaver to remove the covalently grafted species, restoring pristine HOPG, in the presence of electrolyte. The quality of the regenerated sp^2 hybridized graphitic surface was demonstrated by the self-assembly of DBV under electrochemical control. The self-assembly of guest molecules only occurred in the degrafted areas. Control over the shape and size of the nanocorrals, combined with the prospect of site-selective supramolecular self-assembly, may lead to strategies for the study of nucleation and domain growth of molecules under electrochemical control. This experimental finding opens a new way to investigate supramolecular self-assembly of n-/p-doping molecules in nanoconfined spaces under electrochemical control towards bottom-up creation of nanoconfined n-/p-doped 2D materials for nanoscale electronics applications.

Acknowledgements

This work is supported by the Fund of Scientific Research – Flanders (FWO), Internal Funds KU Leuven and Belgian Federal Science Policy Office (IAP-7/05). The research leading to these results has also received funding from the European Research Council under the European Union's Seventh Framework Programme (FP7/2007–2013)/ERC Grant Agreement no. 340324 to S. D. F. T. M. T. H. acknowledges financial support through a Marie Skłodowska-Curie Individual Fellowship (EU project 706564 – NGUEC).

Notes and references

1 J. C. Meyer, A. K. Geim, M. I. Katsnelson, K. S. Novoselov, T. J. Booth and S. Roth, *Nature*, 2007, **446**, 60–63.
2 K. S. Novoselov, A. K. Geim, S. V. Morozov, D. Jiang, Y. Zhang, S. V. Dubonos, I. V. Grigorieva and A. A. Firsov, *Science*, 2004, **306**, 666–669.
3 A. K. Geim, *Science*, 2009, **324**, 1530–1534.
4 C. N. R. Rao, A. K. Sood, K. S. Subrahmanyam and A. Govindaraj, *Angew. Chem., Int. Ed.*, 2009, **48**, 7752–7777.
5 P. Sessi, J. R. Guest, M. Bode and N. P. Guisinger, *Nano Lett.*, 2009, **9**, 4343–4347.
6 M. Z. Hossain, M. A. Walsh and M. C. Hersam, *J. Am. Chem. Soc.*, 2010, **132**, 15399–15403.
7 W.-K. Lee, J. T. Robinson, D. Gunlycke, R. R. Stine, C. R. Tamanaha, W. P. King and P. E. Sheehan, *Nano Lett.*, 2011, **11**, 5461–5464.
8 V. Rebuttini, E. Fazio, S. Santangelo, F. Neri, G. Caputo, C. Martin, T. Brousse, F. Favier and N. Pinna, *Chem. – Eur. J.*, 2015, **21**, 12465–12474.
9 V. Georgakilas, M. Otyepka, A. B. Bourlinos, V. Chandra, N. Kim, K. C. Kemp, P. Hobza, R. Zboril and K. S. Kim, *Chem. Rev.*, 2012, **112**, 6156–6214.
10 X. Dong, D. Fu, W. Fang, Y. Shi, P. Chen and L.-J. Li, *Small*, 2009, **5**, 1422–1426.
11 W. J. Yu, L. Liao, S. H. Chae, Y. H. Lee and X. Duan, *Nano Lett.*, 2011, **11**, 4759–4763.
12 B. Li, A. V. Klekachev, M. Cantoro, C. Huyghebaert, A. Stesmans, I. Asselberghs, S. De Gendt and S. De Feyter, *Nanoscale*, 2013, **5**, 9640–9644.
13 H. K. Jeong, K.-j. Kim, S. M. Kim and Y. H. Lee, *Chem. Phys. Lett.*, 2010, **498**, 168–171.
14 J. M. MacLeod and F. Rosei, *Small*, 2014, **10**, 1038–1049.
15 Q. H. Wang and M. C. Hersam, *MRS Bull.*, 2011, **36**, 532–542.
16 J. Greenwood, T. H. Phan, Y. Fujita, Z. Li, O. Ivasenko, W. Vanderlinden, H. Van Gorp, W. Frederickx, G. Lu, K. Tahara, Y. Tobe, H. Uji-i, S. F. L. Mertens and S. De Feyter, *ACS Nano*, 2015, **9**, 5520–5535.
17 G. L. C. Paulus, Q. H. Wang and M. S. Strano, *Acc. Chem. Res.*, 2013, **46**, 160–170.
18 T. Zhang, Z. Cheng, Y. Wang, Z. Li, C. Wang, Y. Li and Y. Fang, *Nano Lett.*, 2010, **10**, 4738–4741.
19 L. T. Nielsen, K. H. Vase, M. Dong, F. Besenbacher, S. U. Pedersen and K. Daasbjerg, *J. Am. Chem. Soc.*, 2007, **129**, 1888–1889.
20 L. Lee, H. Ma, P. A. Brooksby, S. A. Brown, Y. R. Leroux, P. Hapiot and A. J. Downard, *Langmuir*, 2014, **30**, 7104–7111.

21 E. Bekyarova, S. Sarkar, S. Niyogi, M. E. Itkis and R. C. Haddon, *J. Phys. D: Appl. Phys.*, 2012, **45**, 154009.
22 A. Sinitskii, A. Dimiev, D. A. Corley, A. A. Fursina, D. V. Kosynkin and J. M. Tour, *ACS Nano*, 2010, **4**, 1949–1954.
23 P. M. Kirkman, A. G. Güell, A. S. Cuharuc and P. R. Unwin, *J. Am. Chem. Soc.*, 2014, **136**, 36–39.
24 K. Malmos, J. Iruthayaraj, S. U. Pedersen and K. Daasbjerg, *J. Am. Chem. Soc.*, 2009, **131**, 13926–13927.
25 M. Tanaka, T. Sawaguchi, Y. Sato, K. Yoshioka and O. Niwa, *Langmuir*, 2011, **27**, 170–178.
26 T. Menanteau, E. Levillain and T. Breton, *Chem. Mater.*, 2013, **25**, 2905–2909.
27 C. Combellas, F. Kanoufi, J. Pinson and F. I. Podvorica, *J. Am. Chem. Soc.*, 2008, **130**, 8576–8577.
28 Z. Xia, F. Leonardi, M. Gobbi, Y. Liu, V. Bellani, A. Liscio, A. Kovtun, R. Li, X. Feng, E. Orgiu, P. Samorì, E. Treossi and V. Palermo, *ACS Nano*, 2016, **10**, 7125–7134.
29 M. D'Amour and D. Bélanger, *J. Phys. Chem. B*, 2003, **107**, 4811–4817.
30 M. Hinge, E. S. Gonçalves, S. U. Pedersen and K. Daasbjerg, *Surf. Coat. Technol.*, 2010, **205**, 820–827.
31 L. Civit, A. Fragoso and C. K. O'Sullivan, *Electrochem. Commun.*, 2010, **12**, 1045–1048.
32 W. Haiss, H. van Zalinge, S. J. Higgins, D. Bethell, H. Höbenreich, D. J. Schiffrin and R. J. Nichols, *J. Am. Chem. Soc.*, 2003, **125**, 15294–15295.
33 B. Xu and N. J. Tao, *Science*, 2003, **301**, 1221–1223.
34 Z. Li, B. Han, G. Meszaros, I. Pobelov, T. Wandlowski, A. Blaszczyk and M. Mayor, *Faraday Discuss.*, 2006, **131**, 121–143.
35 S. M. Kim, J. H. Jang, K. K. Kim, H. K. Park, J. J. Bae, W. J. Yu, I. H. Lee, G. Kim, D. D. Loc, U. J. Kim, E.-H. Lee, H.-J. Shin, J.-Y. Choi and Y. H. Lee, *J. Am. Chem. Soc.*, 2009, **131**, 327–331.
36 S. Y. Lee, D. L. Duong, Q. A. Vu, Y. Jin, P. Kim and Y. H. Lee, *ACS Nano*, 2015, **9**, 9034–9042.
37 D. Kiriya, M. Tosun, P. Zhao, J. S. Kang and A. Javey, *J. Am. Chem. Soc.*, 2014, **136**, 7853–7856.
38 M. Wilms, M. Kruft, G. Bermes and K. Wandelt, *Rev. Sci. Instrum.*, 1999, **70**, 3641–3650.
39 T. Phan and K. Wandelt, *Int. J. Mol. Sci.*, 2013, **14**, 4498.
40 D.-T. Pham, K. Gentz, C. Zorlein, N. T. M. Hai, S.-L. Tsay, B. Kirchner, S. Kossmann, K. Wandelt and P. Broekmann, *New J. Chem.*, 2006, **30**, 1439.
41 T. H. Phan and K. Wandelt, *Surf. Sci.*, 2013, **607**, 82–91.
42 S. C. S. Lai, A. N. Patel, K. McKelvey and P. R. Unwin, *Angew. Chem., Int. Ed.*, 2012, **51**, 5405–5408.
43 S. F. L. Mertens, A. Bütikofer, L. Siffert and T. Wandlowski, *Electroanalysis*, 2010, **22**, 2940–2946.
44 H. J. L. Xianglin Zhai, T. Tian, T. Randall Lee and J. C. Garno, *Molecules*, 2014, **19**, 13010–13026.
45 W. L. a. F. B. Prinz, *J. Electrochem. Soc.*, 2009, **156**, G125–G128.
46 E. A. Josephs, J. Shao and T. Ye, *Nanoscale*, 2013, **5**, 4139–4143.
47 O. El Zubir, I. Barlow, G. J. Leggett and N. H. Williams, *Nanoscale*, 2013, **5**, 11125–11131.
48 T. B. Creczynski-Pasa, M. A. D. Millone, M. L. Munford, V. R. de Lima, T. O. Vieira, G. A. Benitez, A. A. Pasa, R. C. Salvarezza and M. E. Vela, *Phys. Chem. Chem. Phys.*, 2009, **11**, 1077–1084.
49 V. Borislav, K. Markus, M. Aleksandar, N. Andreas, R. Uroš, J. Djordje, G. Christian, T. Christian and G. Radoš, *Nanotechnology*, 2013, **24**, 015303.
50 J. Plas, O. Ivasenko, N. Martsinovich, M. Lackinger and S. De Feyter, *Chem. Commun.*, 2016, **52**, 68–71.
51 C. Safarowsky, K. Wandelt and P. Broekmann, *Langmuir*, 2004, **20**, 8261–8269.
52 T. H. Phan and K. Wandelt, *Beilstein J. Org. Chem.*, 2014, **10**, 2243–2254.
53 T. Higashi, Y. Shigemitsu and T. Sagara, *Langmuir*, 2011, **27**, 13910–13917.